

Properties of waterborne polyurethane filled with polyphosphazene nanofibers in situ polymerization

Z. P. ZHAO^a, J. J. HU^b, Z. P. ZHOU^b, M. Q. ZHONG^{b,*}

^aZhijiang College, Zhejiang University of Technology, Hangzhou 310024, P.R. China

^bCollege of Materials Science and Engineering, Zhejiang University of Technology, Hangzhou 310014, P. R. China

Novel hybrid inorganic/organic polyphosphazene nanofibers were synthesized in situ polymerization, and the waterborne polyurethane composites based on it were prepared. The structure of nanofibers is investigated by Fourier transform-infrared spectroscopy. The microstructure of the composites is investigated by scanning electron microscope which indicated that the nanofibers were uniformly dispersed and showed good adhesion with matrix. In comparison with it, the Tg and thermal stability of the composites are all increased. Also, the tensile strength and elongation at break of the composites are all improved. The hydrophobic performance of the composites has a significant difference with the filling content increased by investigation on the surface.

(Received March 27, 2015; accepted February 10, 2016)

Keywords: Waterborne polyurethane, Polyphosphazene nanofibers, Synthesis, Properties

1. Introduction

Waterborne Polyurethane (WPU) is one of the most interesting classes of synthetic polymers that have unique properties due to its friendly to the environment as only water evaporates during its drying process [1-4]. They are widely used in coating, adhesive, artificial leather and automatic industries [5-7]. However, its brittle nature and hygroscopicity restrict its application in some advanced fields. Researchers have developed many additives and modifiers to further improve the physical and mechanical performance of the waterborne polyurethane, such as calcium carbonate, pearl shell powders, silica, titania, alumina, montmorillonite and carbon nanotubes (CNTs) [8-11]. Comparison to physical filling, chemical modification is the recognized optimal introduction to form chemical bond with polymer chains that lead to a better effect since the stability of the chemical bond.

In recent years, with the continuously developing and expanding of nanotechnology, preparation of functional polyphosphazene micro/nano materials has gradually been one of the research focuses on the chemistry of polyphosphazene. If combining the scale advantages of micro/nano materials with the superior performances of polyphosphazene materials, it is expected to expand the applications of polyphosphazene materials in high-tech fields.

Cyclomatrix polyphosphazene micro/nano materials based on hexachlorocyclotriphosphazene (HCCP) are a novel class of polyphosphazene function materials, which have the features of simple preparation, mild synthetic

condition and highly cross-linked structure [12-14]. They not only show excellent thermostability, structural stability, and solvent resistance, but also possess the characteristics of remarkable molecular structure designability, template induced self-assembly, and hetero-atoms doped porous carbon precursor. These features endow it with the good prospects of functionalization and application.

Herein, polyphosphazene nanofibers (PZFs) with active hydroxyl groups were prepared via one-step precipitin polymerization directly and incorporation into WPU matrix to obtain WPU/PZFs composites in situ Polymerization. The goal of the work is to explore the feasibility of polymer/PZFs hybrids by investigating the structure and properties of the composites.

2. Experimental procedure

2.1 Materials

Hexachlorocyclotriphosphazene (HCCP) (synthesized as described in the literature)[15] was recrystallized from dry hexane followed by sublimation (60 °C, 0.05 mmHg) twice before use (mp=112.5-113 °C). Isophorone diisocyanate (IPDI; Degussa) was used as received without further purification. Polyether polyols (GE-220A, Yinrui trading Corporation, Guangzhou China) was dehydrated in vacuum for 45 minutes at 105 °C before used. Dimethylol butanoic acid (DMBA; ChangSheng Chemical Corporation, Hebei China) was placed in the oven drying at 105 °C. Acetone, acetonitrile, toluene,

dibutyl amine, Ethylenediamine (EDA), 4,4'-Dihydroxydiphenyl sulfone (BPS) and triethylamine (TEA) were obtained from Sinopharm Chemical Co., Ltd (Shanghai China). TEA and EDA were distilled onto molecular sieves before used. All glassware was dried in an oven under vacuum before use.

2.2 Characterization

FT-IR spectra of all samples were recorded using the polymer granule on a Perkin-Elmer Wellesley MA spectrophotometer. Thermogravimetric analysis (TGA) was performed on a TGA 7 instrument (PerkinElmer) thermal analysis system. Sample weight taken was 2-4 mg. DSC analysis was carried out on a Perkin-Elmer Pyris 2 DSC analyzer (PerkinElmer), and the glass transition temperature of the polyamides is measured during the heating part of the second thermal cycle at a heating rate of 10 °C/min in N₂ atmosphere. The microstructures of samples were recorded using a Cambridge S250MK3 scanning electron microscope (SEM, U.K.). Mechanical properties were conducted on the Shimadzu DZ10KN universal system with a cross-head speed of 50 mm/min. The results reported are the mean values for five replicates. The isocyanate (-NCO) content was determined by chemical titration, which the same method was described in reference [16].

2.3 Synthesis of poly[cyclotriphosphazene-co-(4,4'-sulfonyldiphenol)] nanofibers (PZFs)

TEA (1.42 g, 14.04 mmol) was added to a solution of BPS (1.08 g, 4.68 mmol) and HCCP (0.54 g, 1.56 mmol) in acetonitrile (100 mL). The reaction mixtures were stirred in an ultrasonic bath (50 W, 40 Hz) at 5 °C for 10 min. The gel-like solid produced were obtained by centrifugation and then washed three times using deionized water and acetone, respectively. Finally, the solid was dried under vacuum at 50 °C for 24 h to yield PZFs directly as a hard white agglomeration. A schematic illustration of the method for the synthesis of PZFs is shown in Fig. 1.

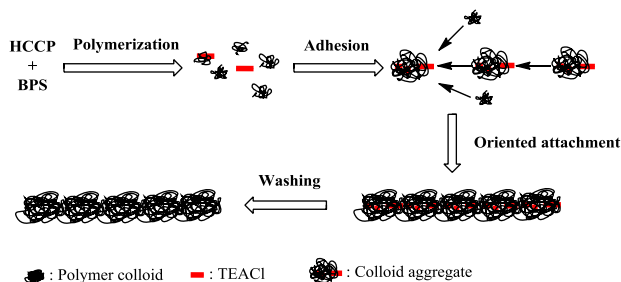


Fig. 1. Schematic illustration of the synthesis mechanism of PZFs nanofibers.

2.4 Preparation of WPU/PZFs composites

The synthetic route of the composites was shown in Fig. 2. At first, a set content of PZFs was dispersed in GE-220A via an ultrasonication for 1 h at room temperature to form a suspension, and then IPDI was added to the suspension and reacted for 1 h at 50 °C. Subsequently, DMBA was added into the flask, and the reaction was carried out for 2h, and then the WPU/PZFs prepolymer was obtained. And the whole reaction was carried out under N₂ flow. Acetone was poured into the flask to reduce the viscosity of the prepolymer and then cooled the temperature to 60 °C. TEA was added as neutralizer, and the reaction was continued for 30 min. Put the diluted solution in distilled water and then emulsify it using the emulsifier at the rate of 4500 r/min. The stoichiometric number of EDA was added to the WPU/PZFs prepolymer (depending on the content of isocyanate groups that are determined using dibutyl amine back-titration method) under a violent stirring condition for 1 h at 40 °C. After that we put the emulsion into PTFE plate for drying solvent, and the WPU/PZFs composites containing about 0 wt.%, 1 wt.%, 2wt.%, 3 wt.%, 4wt.% PZFs were obtained. In the remainder of the article, the abbreviations were marked as WPU-0, WPU-1, WPU-2, WPU-3 and WPU-4, respectively. According to the prepolymer, calculated on the basis of [-NCO]/[-OH]=1.32(mol/mol).

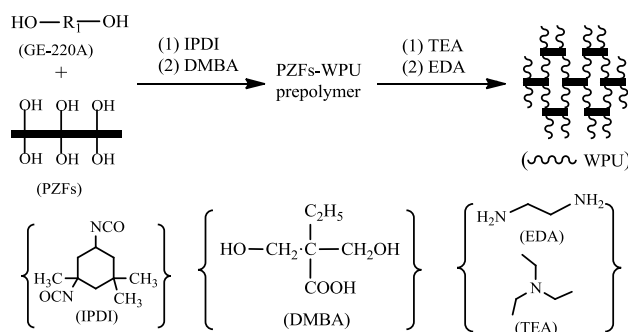


Fig. 2. Synthetic route of WPU/ PZFs composites in situ polymerization.

3. Results and discussion

3.1 Structure of PZFs and WPU composites

The chemical structure of the PZFs was confirmed by FT-IR as shown in Fig. 3. The band at 1478 cm⁻¹ and 1586 cm⁻¹ corresponds to the benzene ring, 1260 cm⁻¹ and 1200 cm⁻¹ are assigned to P=N groups, 940 cm⁻¹ is due to P-O-Ar groups, and the characteristic peaks for O=S=O can be seen at 1290 cm⁻¹. The results demonstrate that the PZFs have the expected chemical structures.

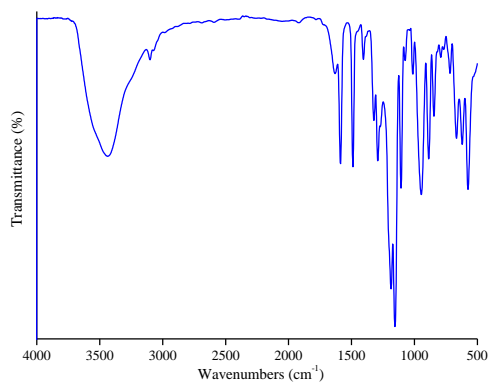


Fig. 3. FT-IR spectra of the PZFs.

The morphology of the PZFs was characterized by SEM are shown in Fig. 4. Fig. 4(a) showed images of bulk and uniform PZFs nanofibers synthesized via a self-directing template plan. The PZFs were with a diameter of 40-60 nm and several thousand nanometers long. The higher-magnification image Fig. 4(b) showed that the surface of PZFs was rather rough with some nanoparticles with an average of several nanometers. Fig. 4(c) and 4(d) are the high resolution TEM photographs of the nanofibers. From the pictures, it is shown that PZFs has no neat structure which indicated that it is amorphous. ED test also indicated that there is a very weak scattering spot in single fibers which could be confirmed the amorphous structure of PZFs.

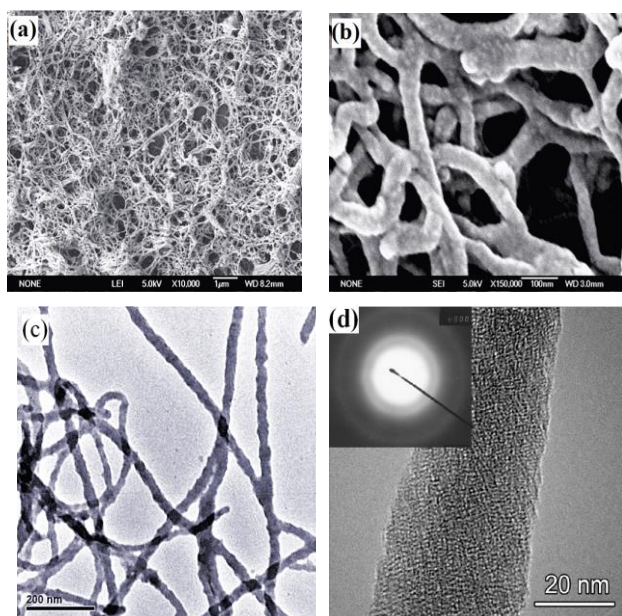


Fig. 4. Field-emission SEM (a, b) and TEM image (c, d) of PZFs nanofibers.

The linkage of PZFs with WPU matrix has been characterized by FT-IR as shown in Fig. 5. All of the spectra show typical absorption bands at 3360 cm^{-1} (N-H Stretch), 2964 cm^{-1} (CH_3 Stretch), 2862 cm^{-1} (CH_2 Stretch), 1692 cm^{-1} (C=O Stretch), 1087 cm^{-1} (C-O Stretch). In

addition, no absorption at 2270 cm^{-1} ($-\text{NCO}$) appears in the spectra, indicated that $-\text{NCO}$ groups in the polyurethane prepolymer had completely reacted with chain extenders. Comparing with others the sample of WPU showed weak absorption at 3360 cm^{-1} . It can be explained by unreacted hydroxyl and $-\text{NH}$ peaks overlap with adding PZFs. The peaks around 1120 and 1100 cm^{-1} are due to C-N and C-O-C bonds stretching, respectively. However, the area ratios of 1220 and 1100 cm^{-1} are different in the five curves. The area ratio of WPU-4 is slight larger than that of WPU-0 which is due to P=N stretches (1200 cm^{-1}) of PZFs existing in WPU-4.

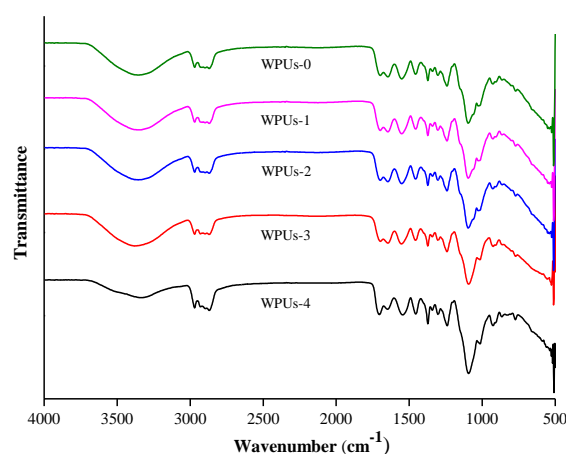


Fig. 5. FT-IR spectra of the composites.

The dispersion of PZFs greatly affects the properties of the composites. Thus, the dispersion of its in the matrix fracture surface was examined by SEM as shown in Fig. 6. From the microscopic morphology, it can see that PZFs dispersed well in the matrix when the low filler content. It is showing that PZFs have a good compatibility with the matrix and no obvious cracks and flaws. But the difference is the distribution density. However there are few of clusters observed.

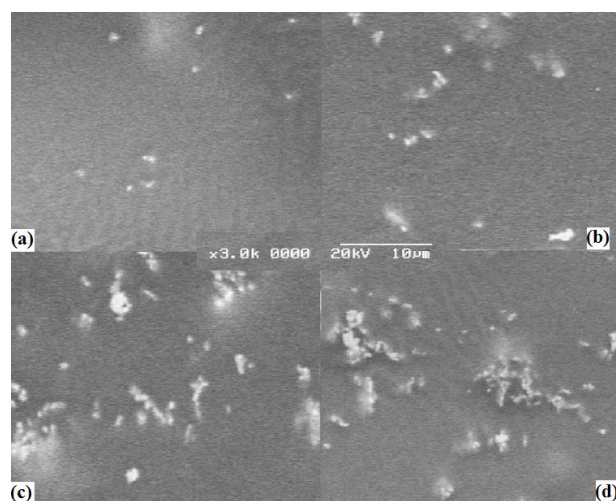


Fig. 6. Microscopic morphology of the composites: (a) WPU-1, (b) WPU-2, (c) WPU-3 and (d) WPU-4.

3.2 Properties of the WPU composites

The thermal properties of the samples were examined by investigating the thermal stability and glass transition temperature (T_g). The thermal stability of samples was evaluated using TGA (Fig. 7). PZFs had a better thermal stability than the WPU samples. In addition, the initial temperature of degradation and maximum degradations were all obviously higher than pure WPU. The significantly improved thermal stability of the composites could be attributed to adding PZFs. PZFs consisted cross-linking structure of itself and the composites which could quickly transfer the heat from the matrix to the PZFs nanofibers to ensure that the heat distribution is uniform through the composites, avoiding that the materials are ahead decomposed due to excessive heat in local. All samples occur weight loss twice. The first one corresponded to the decomposition of soft segment at about 220 °C. The other one corresponded to the decomposition of hard segment at about 300 °C. Weight loss corresponds to water evaporation before 100 °C.

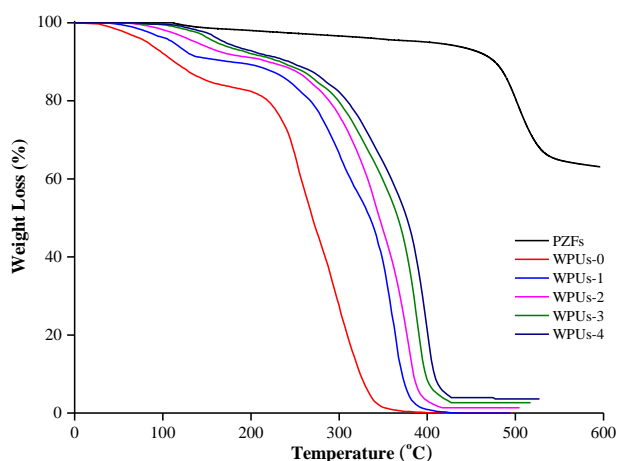


Fig. 7. TGA curves of WPU/PZFs composites.

From the DSC curves (Fig. 8), it is shown that the glass transition region shifted toward higher temperature with increasing PZFs content. The WPU-s-0 has two T_g from -50 °C to 30 °C. The first transform corresponded to the movement of soft segment and the other corresponded to the movement of hard segment. The PZFs were easy to gather due to hydrogen bonding interactions between molecules. Homogeneous structure was destroyed by adding PZFs leading to showing two T_g . Thus adding PZFs was conducive to phase separation in the WPU. The modified WPU had a higher T_g because the cross-linking made the segment move difficult. A little PZFs nanofibers uniformly disperse in the composites and the polyurethane molecular chains wrapped around the

nanofibers to form a solidly reinforced frame, which can effectively limit the movement of the polymer chain at heating condition, thereby improving the T_g . Meanwhile, the large number of hydroxyl-rich surface of the nanofibers can form hydrogen bonds with molecular chains to enhance the interface combination between the nanofibers and the matrix. PZFs play a role in chemical crosslinking points, increase the crosslinking density and improve the T_g .

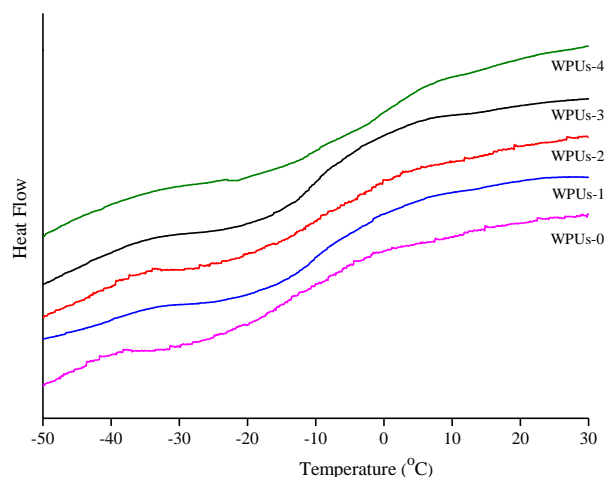


Fig. 8. DSC curves of WPU/PZFs composites.

Fig. 9 shows the tensile strength and elongation at break of WPU composites respectively. From the curves, it is indicated that the tensile strength of the modified WPU composites increased significantly compared with the pure WPU. It may be attributed to the cross-linking structure of the bonds of matrix polymer and organic-inorganic hybrid nanofibers. The tensile strength could be quickly transferred from the WPU matrix to the full cross-linked nanofibers. So the PZFs could be deformed to distribute strength through the composites avoiding that the materials are ahead fracture due to excessive strength in local. A certain level of cross-link can increase the interaction between polymer chains. Physical entanglement also occurred between the molecular of WPU and PZFs. Some crossing point can prevent the slippage of molecular chains that increase the elongation at break. When the degree of cross-linking is greater than a certain level, the polymer will become brittle. Defects caused by phase separation could lead to a decline in the elongation at break, too. Therefore, the elongation at break of WPU-s-4 reduced to some extent from the cruves.

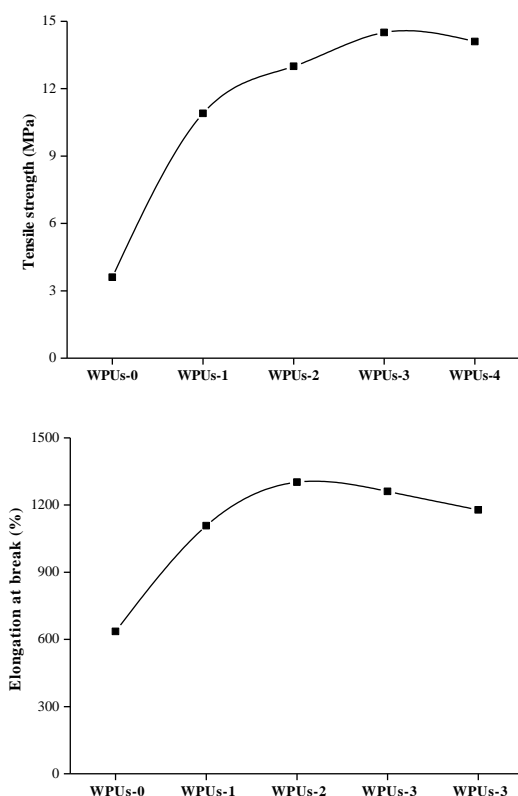


Fig. 9. Tensile strength and elongation at break of the composites.

Water contact angle measurements were examined to demarcate the surface hydrophobicity of the composites. The data are summarized in Table 1. The water contact angle of pure WPU was 61.3° , increased by 26° of the WPU-2 and 40° of the WPU-4, respectively. There are significant improvements in it. It is likely to be because PZFs has much more hydrophobic aryloxy groups and belongs to the high degree of crosslinking polymer. Therefore, it is showed that the composites were more hydrophobic than WPU.

Table 1. Water contact angles of WPU/PZFs composites.

Sample	Water Contact Angle
	$^\circ$
WPU-0	61.3
WPU-2	87.9
WPU-4	101.4
PZFs	127.2

4. Conclusions

A series of novel WPU hybrid composites based on PZFs were successfully fabricated in situ Polymerization. The chemical structures of the PZFs and WPN/PZFs composites were confirmed by FT-IR and the microstructures were also examined by SEM. The properties of the composites were characterized by TGA, DSC, tensile testing and water contact angle measurements. PZFs nanofibers have an average diameter of 40-60 nm and several thousand nanometers long and excellent thermal stability. PZFs nanofibers could be dispersed well in the WPU matrix. The T_g and thermal stability were improved with the increasing content of PZFs in comparison with WPU. PZFs nanofibers were also improved the tensile strength and elongation at break due to the formation of cross-linking structure. The WPU/PZFs composites were more hydrophobic than pure WPU through comparing the water contact angle. This work is possible to exploit a novel series of WPU/PZFs nano-composites.

Acknowledgements

We are thankful for the National Natural Science Foundation of China (No. 21504079) and Project Supported by Zhejiang Provincial Natural Science Foundation of China (Grant No. LQ14E030004) for the support to this research.

References

- [1] J. Y. Li, W. Zheng, W. B. Zeng, D. Q. Zhang, X. H. Peng, *Appl. Surf. Sci.* **307**, 255 (2014).
- [2] Z. Z. Gao, J. Peng, T. H. Zhong, J. Sun, X. B. Wang, C. Yue, *Carbohydr. Polym.* **87**, 2068 (2012).
- [3] X. H. Hu, X. Y. Zhang, J. Liu, J. B. Dai, *J. Lumin.* **142**, 23 (2013).
- [4] D. Macocinschi, F. Miculescu, S. I. Voicu, *Optoelectron. Adv. Mat.* **5**, 677 (2011).
- [5] M. Akbarian, M. E. Olya, M. Ataefard, M. Mahdavian, *Prog. Org. Coat.* **75**, 344 (2012).
- [6] J. Huybrechts, P. Bruylants, A. Vaes, A. De Marre, *Prog. Org. Coat.* **38**, 67 (2000).
- [7] H. Liu, S. Q. Cui, S. B. Shang, D. Wang, J. Song, *Carbohydr. Polym.* **96**, 510 (2013).
- [8] Z. H. Fang, H. Y. Duan, Z. H. Zhang, J. Wang, D. Q. Li, Y. X. Huang, J. J. Shang, Z. Y. Liu, *Appl. Surf. Sci.* **257**, 4765 (2011).
- [9] Y. L. Lin, Y. Zhou, C. X. Xu, A. D. Xie, M. H. Yang, S. Yang, H. X. Chen, *Prog. Org. Coat.* **76**, 1302 (2013).
- [10] S. J. Lee, B. K. Kim, *Carbohydr. Polym.* **87**, 1803 (2012).

- [11] Z. F. Wu, H. Wang, X. Y. Tian, M. Xue, X. Ding, X. Z. Ye, Z. Y. Cui, *Polym.* **55**, 187 (2014).
- [12] H. R. Allcock, J. L. Desorcie, G. H. Riding, *Polyhedron* **6**, 119 (1987).
- [13] R. James, M. Deng, S. G. Kumbar, C. T. Laurencin, *Nat. Synth. Biomed. Polym.* **6**, 193 (2014).
- [14] N. R. Krogman, A. L. Weikel, K. A. Kristhart, S. P. Nukavarapu, M. Deng, L. S. Nair, C. T. Laurencin, H. R. Allcock, *Biomater.* **30**, 3035 (2009).
- [15] Z. P. Zhao, Q. Guo, X. Li, J. L. Sun, Z. J. Nie, *Express Polym. Lett.* **6**, 308 (2012).
- [16] I. E. Raschip, L. Moldovan, L. Stefan, *Optoelectron. Adv. Mat.* **3**, 1336 (2010).

*Corresponding author: sjzhaolei@163.com